Department of Metallurgy and Materials Science
Massachusetts Institute of Technology
Cambridge, Massachusetts

RESEARCH ON MECHANISMS OF ALLOY STRENGTHENING

I. Alloy Strengthening by Fine Oxide Particle Dispersion

II. The Splat Cooling Process for Alloy Development

Semi-Annual Report

December, 1967

NsG 117-61, Supplement 6

Submitted by:

Nicholas J. Grant, Supervisor

Research Associate:
Bill C. Giessen

Research Assistants:
Harish Dalal
Gary Ewell
Francis Hunkeler
Christina Jansen
William Schilling
Manohar Singh
Michael Lebo

To:

National Aeronautics and Space Administration
Washington, D. C. 20546

INTRODUCTION

To restate the two major aims of this program, it was intended:

(1) to study oxide dispersed alloys to establish the mechanisms of strengthening, to examine the modes of deformation and fracture, and to examine new or different processing techniques whereby structures could be improved, stability enhanced, and processing steps made simpler and more readily controllable;

(2) to undertake studies to determine the potential of rapidly quenched, atomized or splat cooled particles as a basis for the development of improved or new alloy systems.

During the latter half of 1967 and the early part of 1968, a number of studies which had been initiated about three years earlier reached a stage where they can be considered as complete items of research. One Sc. D. thesis has been submitted and approved, and a second will have been approved in February, 1968. The results of these studies will be summarized below, and conclusions based on these studies will be listed in each category.

In addition, all of the other research programs have advanced in important ways so that fairly extensive data are now available to show trends and possibly to permit preliminary conclusions.

This report is concerned primarily with the results achieved during the last six months of 1967; preliminary results which were reported in the semiannual report through June 1967 will not be repeated .

I. ALLOY STRENGTHENING BY FINE PARTICLE DISPERSION

A. Oxide Dispersed Iron-BeO Alloys

A doctoral thesis has been accepted covering the work on this alloy system, signifying essentially that a unit of work has been completed and is deserving of publication consideration.

By way of a brief review, a series of -325 mesh alloy powders of increasing Be content in Fe was internally oxidized at 800°C; the powders were hydrogen reduced, compacted, and extruded into bar stock. The resultant beryllium oxide contents were about 0.75, 3, and 6 volume percent BeO. A fourth alloy was subjected to extensive attritor grinding, resulting in sub-micron thick flakes, which were surface oxidized to produce a thin layer of BeO on each powder flake; the iron oxide on these flakes was hydrogen reduced, the powders were compacted in a mild steel can, and were then extruded to produce an alloy of iron with a small but significant amount of beryllium in solid solution, and containing approximately 2.5 percent BeO.

Of particular importance, the powder used to produce the three volume percent BeO alloy was split into two sections after internal oxidation; one batch was extruded in the ferritic temperature range, and the second was extruded in the austenitic temperature range. It was expected that the austenitic extrusion would have both a different grain size and be fully recrystallized as a result of cooling through the transformation temperature.

Figure 1 shows the log stress versus log rupture time plots for all of the Fe-BeO alloys, tested in the as-extruded condition, at a test temperature of 1200°F. Alloy E with only 0.75% BeO shows a relatively steep slope. Alloys B and C with 3% BeO show excellent flat slopes; B was extruded in the ferritic temperature range, and C was extruded in the austenitic temperature range. It will be observed that while both curves are quite parallel, the ferritic extrusion is stronger at all stresses than the austenitic extrusion. Alloys F and J, both containing about 6% BeO, are considerably stronger than B and C, and show the desired flat slopes in the stress vs. rupture time plot. Alloy L, which contains a small amount of beryllium in solid

solution, has 2.5% BeO; it is very much stronger in short time tests than the other alloys, but seems incapable of maintaining this strength in long time tests. The relatively rapid decrease in load carrying capacity of this alloy is not understood as of now.

Figure 2 is particularly interesting. It is a plot of log stress versus log rupture time for the B and C alloys, containing 3 volume percent BeO. Curve B is the alpha extrusion and shows the highest strength values. Curve C, the gamma extrusion, lies parallel to the B curve but displaced from it by about 2000 psi.

a) If one now takes the ferritic extrusion, B, and reheats it to 1720°F in the gamma range, for about one hour, the resultant test points fall on the same curve as that occupied by alloy C, the gamma extrusion. Heating of the B material into the austenitic range has resulted in a significant decrease in strength.

b) If one takes the gamma extrusion, C, and subjects it to a second exposure in the gamma range at 1720°F, the rupture life curve now falls to a new lower position; see curve C(T).

c) Similarly, if one takes the alpha extrusion, B, and cold works it at room temperature by 28% reduction of area, and heats it in the gamma range to 1720°F, these values also fall on the same curve as the C(T) condition, a further weakening.

d) Finally, if one takes the gamma extrusion, C, cold works it at room temperature by 15% reduction of area, and reheats it to 1720°F in the gamma range, the properties fall to the lowest recorded values; see curve CS(T).

It is clear that the ferritic extrusion is the strongest of the group; exposure of the B alloy, or re-exposure of the C alloy above the transformatinn temperature results in a significant loss of strength. In particular, cold work of either the B or C alloy at room temperature, followed by exposure at 1720°F in the gamma range, results in further losses of strength. In all these instances, recrystallization has resulted in weakening of the as-extruded product.

Equally important and interesting is the very flat slope of all of the curves, even after recrystallization, in the log stress - log rupture time plot. Thus, while the strength levels are decreased, the alloys continue to show large improvements in long life tests compared to conventionally strengthened alloys, a characteristic of oxide dispersed alloys. This same behavior has been observed in the past, but a clear-cut explanation had not been available.

Examination of the microstructures of these alloys reveals that the alloys all have discrete stringers of BeO particles; the stringers result from preferential grain boundary oxidation during internal oxidation. The material in between the prominent oxide stringers has various degrees of oxide stringering, including many isolated, uniformly dispersed oxides. These oxide particles have the capacity to pin grain boundaries such that the boundaries tend to be square sided instead of being of usual polygonal shapes.

The distribution of the BeO particles is such that grain boundaries lie parallel to the extrusion direction, and therefore parallel to the tension axis in the stress rupture test; the boundaries are confined in this position, which is a non-sliding direction. The transverse boundaries in this structure are sharply jagged in short lengths, and are pinned by discrete BeO particles distributed between the heavier oxide stringers. This means that at no time is there any significant length of grain boundary which offers easy sliding in easy shear directions. Since sliding cannot occur easily, and is restricted to very short distances by the pinning with oxide particles, grain boundary shear activity is extremely limited, grain boundary migration obviously must be limited, and the usual equi-cohesive break in the log stress - log rupture time plot is avoided. This accounts for the extremely flat slopes of the curves in Figure 2, regardless whether the curves are for the cold worked (as-extruded) condition, or whether they are in the recrystallized condition.

It was fortunate that these iron alloys, with a grain size of 20 - 50 microns, responded to simple etching techniques which revealed these boundaries. It has always

been a problem in the past that the very fine grain structure of the oxide dispersed alloys was seldom capable of being revealed and studied. It is now clear from the previous work of Adachi and Grant, and the extensive works reported on TD-nickel, that the flatness of the slope, even in the recrystallized condition for these alloys, is associated with the restriction of grain boundary sliding, which is a weakening process, and therefore results in excellent long-time stress rupture properties.

In examining the fractures of these materials, fracture starts only on the jagged transverse boundaries, on those sections inclined at some preferred angle near 45° to the strain direction; many short crack lengths are ultimately formed, and then interconnect by subsequent shear on less favorably oriented boundaries, including the vertical short lengths. Examination of the final fractures indicates many fine shear cracks with the general crack direction being normal to the specimen axis and to the extrusion direction.

Figure 3 compares the 1200° stress rupture properties of alloys B (3% BeO) and J (6% BeO) with the two best known ferritic stainless steels over the temperature interval 1000, 1200, and 1400°F. The following observations may be made:

1) At 1000°F, the conventional heat treated ferritic stainless steels are quite strong, and are superior to the oxide dispersed alloys over all levels of stress studied. At 1000°F these alloys undergo only transgranular fractures.

2) At 1200°F, in longer time tests, the oxide dispersed materials being to show large superiority over the ferritic stainless steels, primarily because of the absence of the equi-cohesive break in the oxide dispersed materials. The relatively strong and fine structure of the ferritic stainless steels coarsens in longer time tests at this temperature. These conventional alloys are subjected to extensive grain boundary shear and migration, and suffer rapid loss of load carrying capacity with decreasing stress.

3) While it is certainly not anticipated that these pure iron base materials could be used for significant periods of time at 1400°F in an oxidizing atmosphere, nevertheless tests were run to establish the load carrying capability of the structure. It will be observed that at 1400°F the oxide dispersed Fe-BeO materials are superior at all stress levels to the best known ferritic stainless steels, and show excellent engineering strength values.

It was anticipated that the Fe-BeO alloys were suffering from oxidation, and therefore not showing optimum stress rupture performance at 1400°F. Accordingly, a small number of tests were run at 1400°F with the iron-BeO, B, alloy in the chromized condition, which provided adequate oxidation protection for the periods of time utilized for these tests. It will be observed in Figure 4 that the slope of the chromized Fe-BeO alloy is significantly more flat than that of the unprotected material. The curve for the chromized alloy shows the actual strength of this material, and suggests that Fe-Cr-BeO alloys should be interesting alloys for this temperature range.

These results show clearly that the body-centered-cubic iron base materials are capable of being strengthened in large measure for long-time service up to at least 1400°F, if oxidation protection can be provided. The alloys are expected to be from 3 to 6 times stronger (in terms of stress) than are the best conventional alloys now available.

A technical report of this work is being prepared to provide a more complete disclosure of the results obtained.

B. Oxide Dispersion Strengthened Copper-Al_2O_3 by the SAP Technique

Excellent progress and interesting results may now be reported on this series of alloys, and preliminary conclusions will be drawn.

These alloys were prepared from -44 micron atomized copper-aluminum alloys which had been attrited for a period of about six hours in ethanol to produce a flake product of thickness less than 0.5 micron with length and width dimensions between about 3 and 5 microns. The alloy was air oxidized in the course of comminution, forming both copper oxide and thin films of aluminum oxide on the surface of the thin flakes. In the first series of alloys, discussed here, the surface copper oxide is reduced, leaving only Al_2O_3 on the surface, after which the flake material is compacted in a can, evacuated, sealed, and extruded at 740°C. Subsequent alloys, in a second series, utilize the surface copper oxide to achieve by internal oxidation an increase in the total aluminum oxide content and improve the oxide dispersion. With the higher alumimum containing alloys the amount of internal oxidation will be very small.

The maximum extrusion pressure was about 720 tons, and the average was about 640 tons. Density measurements show that the alloys were better than 99.7% dense, a figure considered to be satisfactory for these materials.

Thus far, three alloys have been extruded and tested fairly extensively. The compositions and extrusion ratios of these alloys are shown in Table I.

TABLE I

Compositions* and Extrusion Ratios

Alloy No.	Wt. % Cu	Wt. % Al	Wt. % Al_2O_3	Vol.% Al_2O_3	Extru. Ratio
A1	98.3	0.65	0.63	2.3	12:1
A2	96.0	2.80	0.87	2.9	22:1
A3	91.95	6.86	1.42	4.5	22:1

* Determined from the extruded bar. In each alloy there is aluminum remaining in solid solution in the copper.

All three alloys extruded satisfactorily. Conventional light microscopy has indicated that the structures are excellent and that relatively uniform dispersions of alumina have been obtained in all cases. Thus far, measurements of the particle size and interparticle spacing have not been made quantitatively, but are planned.

Room temperature tension properties are summarized in Table II, and are compared with three previously reported copper-alumina alloys. Alloys B-23 and B-33 are from the work of Preston and Grant and are the strongest oxide dispersion strengthened alloys produced to date, by internal oxidation of dilute Cu-Al alloys. The third of these alloys, G, represents the best properties reported for an alloy prepared by mechanical mixing, from the work of Zwilsky and Grant. Alloy G was made from 1 micron copper containing 7.5 volume percent Al_2O_3 added as 0.018 micron particles. The B-23 and B-33 alloy extrusion ratios were 28:1, for the G alloy it was 20:1.

TABLE II

Room Temperature Tension Properties for As-extruded Condition

Alloy	0.2% Y.S., psi	U.T.S., psi	Elong. %	Reduction Area, %
A1	46,200	49,700	19.8	22.6
A2	53,400	59,600	19.6	26.4
A3	83,100	92,600	7.5	10.5
B-23 (1)	58,200	68,000	19.0	54.0
B-33 (1)	65,100	76,000	13.0	31.0
G (2)	69,900	88,500	5.0	7.0

(1) From Preston and Grant: Cu-1.1 v/o Al_2O_3 and Cu-3.5 v/o Al_2O_3 by internal oxidation.

(2) From Zwilsky and Grant: Cu-7.5 v/o Al_2O_3 by mechanical mixing

The lower test values for alloys A1 and A1 compared to A3 can be accounted for in terms of the lower aluminum and aluminum oxide contents, and in the case of alloy A1 also by the considerably lower extrusion ratio. Alloy A3, with a higher oxide content and an extrusion ratio of 22:1, shows excellent room temperature tension properties; part of this strength is attributable to the fairly large amount of aluminum remaining in solid solution. Alloy A3 is considerably stronger than B-33, and importantly stronger

than alloy G, while enjoying improved ductility at the same time over the G alloy.

One of the purposes of this program was to study the effect of additional cold work at room temperature (after hot extrusion) on both the low and high temperature properties of these alloys. Accordingly, alloy A1, with the lowest oxide content, was extruded at a relatively low extrusion ratio in order to provide a material which would have a larger capacity for subsequent cold work. In parallel studies, alloys A2 and A3 will be examined for their capacity for subsequent cold work. It is anticipated that the level of additional cold work in the higher oxide, higher extrusion ratio alloys will be relatively small, although beneficial effects are expected. Among other features, it is expected that alloy A1 will develop a stronger texture as a result of the low oxide content and larger amount of cold work it will undergo; it is intended to examine the effects of the resultant texture on properties.

The stability of these alloys has been checked by room temperature hardness measurements after a one hour exposure at progressively higher temperatures up to 1000°C. This type of hardness survey has been indicated to be a suitable preliminary means of checking the alloys for further high temperature testing.

Figure 5 shows the hardness as a function of a one hour annealing treatment at high temperatures. Results are compared with alloys B-33 and G to provide a suitable base line. Figure 5 clearly shows the higher hardness levels of alloys A1, A2, and A3 because of the benefits derived from solid solution strengthening of the copper by aluminum. Of the three alloys, A1 loses hardness more rapidly than the other two materials, and also more rapidly than alloys B-33 and G. Alloys A2 and A3 show excellent stability in terms of hardness, and it is expected that this stability will be manifested also in the stress rupture tests.

The stress for a 100-hour life at 450 and 650°C for alloys A1, A2, A3, B-23, and B-33 are shown in Table III. It is clear that alloy B-33 continues to show the best strength values at both 450 and 650°C. This undoubtedly represents the much more ideal dispersion of Al_2O_3 in the completely internally oxidized alloy, as compared to the surface oxidized flake materials.

TABLE III

Stress for 100-hour Life at 450 and 650°C. Tests in Air

Temp. °C	Alloy No.	Stress for 100-hour life, psi
450	A1	19,000
	A2	23,000
	A3	25,000
	B-23	31,000
	B-33	38,000
650	A1	8,500
	A2	13,500
	A3	14,800
	B-23	16,000
	B-33	21,000

It would appear from these results that the aluminum in solid solution is not especially beneficial to stress rupture properties when the temperature is as high as 450°C or greater. This tends to confirm tests with alloyed aluminum SAP and some modified TD-Ni alloys at high homologous temperatures.

Even though alloy A3 has lower strength properties than B-33, the results are nevertheless excellent when compared to all other known high temperature copper materials. Further, the drop in strength for the A3 alloy on increasing the test temperature from 450 to 650°C is significantly less than that for the B-23 and B-33 alloys.

One advantage of the A series of alloys reported here is that they have excellent oxidation resistance at 450° and 650°C. In particular, alloy A3, with its higher residual aluminum content, has excellent oxidation resistance for long-time periods at 650°C.

The amount of work done to study the effects of additional cold work on the strength properties of these alloys is fairly limited. Alloy A2 was cold swaged to give a reduction in cross sectional area of about 50 percent. Table IV shows the results of the comparative room temperature tensile data for the as-extruded material and the cold worked material. It will be observed that cold working has increased significantly the strength values, with a resultant loss in ductility, which does not

appear too severe. Creep rupture tests are also planned to see whether the benefits of the cold work are maintained at the high test temperature.

TABLE IV

Room Temperature Tension Properties for Cold Worked Alloy A2

Condition	0.2% Y.S., psi*	U.T.S., psi	Elong., %	Reduction Area,%
As extruded (22:1)	53,400	59,600	19.6	26.4
Cold swaged, 50% RA	86,100	86,500	12.6	13.2

* Instron: cross head speed of 0.05" min^{-1}

Surface Plus Internal Oxidation Series

A second series of copper-aluminum alloys also in fine flake form (B series) is being processed by internal oxidation following surface oxidation. It was anticipated that the aluminum oxide dispersion could be improved by the additional oxidation of aluminum to Al_2O_3. Accordingly, the fine flake powders of sub-micron thickness, described above having both copper oxide and aluminum oxide on the surface, were internally oxidized for one hour at 725°C. Calculations from prior literature had indicated that these fine powders could be thoroughly internally oxidized within two or three minutes; however, because of difficulties in bringing the system up to temperature, controlling the temperature for a short interval of time, and ascertaining that penetration of the oxidizing atmosphere through the powder mass would be uniform, the powders were actually internally oxidized for the considerably longer time of one hour. Table V shows the initial and final compositions of the four alloys being studied.

TABLE V

Composition of Alloys after Surface plus Internal Oxidation

	Weight Percent				Volume Percent
Alloy*	Cu	Al	Al_2O_3	Ni	Al_2O_3
B1	98.3	0.58	0.80	-	2.9
B2	95.4	2.65	1.27	-	4.2
B3	91.4	6.89	1.34	-	4.5
B4	84.3	0.06	1.22	14.71	4.4

* Initial powder compositions same as for A series of alloys

The B series represents higher levels of Al_2O_3 for alloys B1 and B2 compared to A1 and A2 (Table I), but comparable Al_2O_3 contents for B3 and A3, which had such a high level of aluminum in solution that internal oxidation is largely restricted.

Finally, Table VI lists the results of all stress rupture tests to date on alloys A1, A2, and A3, and summarizes the stress to produce rupture in 100 and 1000 hours at 450, 650, and a few tests at 850°C.

TABLE VI

Results of Creep-Rupture Testing - All Tests in Air

Alloy	Temp. °C	Stress, psi	Rupt. life, hrs.	Elong., %	Reduction Area,%
A1	450	22,500	0.36	4.6	5.1
		20,000	16.7	4.3	2.4
		18,000	> 454.6	2.5	2.4
	650	15,000	0.05	5.0	2.4
		12,500	2.02	3.3	2.4
		10,000	35.5	5.4	1.2
		9,000	60.2	-	2.4
		8,000	380.	3.3	3.9
A2	450	25,000	1.38	7.1	5.1
		24,000	16.3	6.2	3.9
		23,000	25.8	6.6	2.6
		22,500	373.6	4.4	2.4
	650	15,000	0.31	5.1	3.9
		14,000	16.4	3.3	3.9
		12,500	516.0	4.4	5.1
A3	450	29,000	0.026	5.8	7.1
		28,000	0.24	20.4	23.4
		27,450	48.5	3.8	6.3
		25,000	82.5	6.4	13.9
	650	20,000	0.127	5.7	7.8
		17,000	3.08	4.5	5.5
		15,000	40.7	5.1	11.7
		14,000	90.7	2.6	4.8
	850	10,000	0.003	24.2	33.2
		8,000	0.01	18.3	40.0
		4,000	15.3	-	3.9

TABLE VI (Continued)

Alloy	Temp. °C	Stress for 100 hr. life (est.)	Stress for 1000 hr. life (est.)
A1	450	19,000	17,500
A2		23,000	21,800
A3		25,000	23,500
B-23		31,000	28,000
B-33		38,000	37,000
G		21,800	20,400
A1	650	8,500	7,800
A2		13,500	12,700
A3		14,800	13,500
B-23		16,000	12,000
B-33		21,000	19,000
G		11,200	9,500
A3	850	3,600	2,200
B-33 (1)		8,000	6,600

(1) test in argon

C. The Role of Oxide Contaminants and Reactive Metals in Oxide Dispersed Alloys

In the June semi-annual report, two type 316 stainless steel alloys containing 5 volume percent thoria were discussed; the alloys were prepared by mechanical blending. The starting 316 powders were of the -10 micron size. In the course of preparing these materials, high temperature hydrogen reduction treatments were used to reduce Cr_2O_3; this gave two slightly different products, one containing 1.23 and the other 0.90 weight percent Cr_2O_3. Hardness measurements had indicated that the alloys began to recrystallize at about 2000°F after one hour exposure, but had shown only a small drop in room temperature hardness after annealing at temperatures up to 2300°F. On this basis, it had been hoped that the creep rupture properties might be rather good; instead, the stress rupture results were quite poor, each alloy showing a stress of about 1500 psi for a 5 hour rupture time at 1800°F.

It would appear that room temperature hardness measurements after a one hour exposure at high temperatures are not always a good measure of the strength values to be achieved in alloys of this type. The chromium oxide content was relatively high, the ThO_2 dispersion only fair at best. It is anticipated that the stress rupture properties were poor in part because of this chromium oxide contamination.

Two oxidation resistant, chromium containing alloys had been received which were of considerable interest because they had been made by the ONERA halide decomposition process. The two alloys received as pressed compacts were:

1) 80 Ni - 20 Cr - 3.5 ThO_2

2) 80 Fe - 20 Cr - 3.5 ThO_2

As indicated below, these alloys also showed relatively good stability when judged in terms of room temperature hardness versus a one-hour annealing treatment at progressively higher temperatures.

TABLE VII

One Hour Annealing Temperature, °F	Hardness Rockwell, G	
	Ni-Cr-ThO_2	Fe-Cr-ThO_2
As-extruded	98	78
1800	96	78
2000	96	77
2300	92	74
2500	90	63

The hardness data suggest that the austenitic nickel-chromium-thoria alloy is not only harder (stronger) but is also more stable than the iron-chromium-thoria alloy.

In tension tests at room temperature, the nickel-chromium alloy showed excellent properties, having a yield stress of 113, 700, an ultimate tensile strength of 126,200 psi, and an elongation of 6.7%. The iron-chromium-thoria alloy showed relatively low stregth values, having a yield strength of 53,700 psi, an ultimate tensile strength of 75,000, and an elongation of 8.7%.

Again unfortunately the creep rupture properties were very poor. The results were actually lower than those for the type 316 stainless steels with mechanical admixtures of thoria.

Metallographic examination indicated that something had gone seriously wrong during the halide decomposition process since the chromium in the alloys was not homogeneously distributed in the structure. This left large islands of a chromium-rich phase which was susceptible to extensive diffusion in the high temperature treatments, yielding a unstable structure.

Because of the excellent structure and properties obtained with our Fe-BeO alloys produced by internal oxidation (described above), a quantity of this material in the form of -44 micron internally oxidized powder was subjected to a chromizing treatment by the halide process. The resultant composition is indicated to be Fe-19 Cr - 2.5 BeO. Room temperature tension tests with this alloy show a yield strength of 72,500 psi, an ultimate tensile strength of 104,000 psi; an elongation of 16.6%. These results are excellent and considerably better than those for the iron-chromium-thoria alloy produced

completely by the halide process and described above.

Initial stress rupture tests will be made at 1400°F with this alloy to see how they compare with a straight Fe-BeO alloy, free of chromium, which showed promising results up to 1400°F. If these results look attractive, tests will be continued at 1800°F.

In addition to the chromium containing alloys which are being studied to determine the stability of the alloys in the presence of a reactive solute element such as chromium, a number of copper alloys are also being examined. Two of these alloys contain significant amounts of aluminum in solid solution. Accordingly, these copper-aluminum-Al_2O_3 alloys are being studied for structural stability in the same way as the nickel-chromium and iron-chromium dispersion strengthened materials. Coarsening rates for the oxides for all of these alloys will be compared with the results for the same alloy systems free of the reactive solute element.

A new series of alloys have been prepared by the halide process, taking into account the previous problems with chromium solution in the matrix. These alloys have been received and are scheduled to be extruded preparatory to mechanical testing.

D. Deformation and Fracture of Dispersed Oxide Alloys

For this study, a range of alloy types and compositions were obtained from within the laboratory in order to try to cover as many aspects of the deformation and fracture study as possible. Included in the study were SAP alloys, internally oxidized copper-aluminum oxide alloys, nickel-thoria alloys, and internally oxidized Fe-BeO alloys.

Test conditions included tension tests at room temperature and 77°K, and stress rupture tests at elevated tempratures. Both light microscopy and electron microscopy were utilized. In the latter case, only replication techniques were used, but the studies included both external surfaces as well as fracture surfaces.

The following observations and conclusions are made as a result of this study;

1) Slip traces observed on the surface of oxide dispersed alloys, in the pre-polished conditions, in tests at room temperature and 77°K, were predominantly of the fine slip variety. The Cu-Al_2O_3 alloys showed similar slip traces to those observed

in over-aged, precipitation hardened aluminum alloys. Similarly, slip traces in Fe-BeO alloys are quite similar to those found in pure iron at low temperatures. Slip bands are almost never seen; actually, it is difficult to conceive how slip bands might form in structures containing a fine dispersion of hard oxide particles. Fine slip, which accounts for most of the deformation anyhow, is readily blocked by the oxide particles, however, the slip may be reactivated on the opposite side of the same particle. Frequently the slip traces at high magnifications looks quite jagged as deformation proceeds around the hard particle.

It should be pointed out that in most cases the oxide dispersed alloys which were examined had a grain size which was so fine that accommodation of slip bands would be difficult, in line with the Orowan relationship between stress and the inverse of the slip band spacing. For a very fine grain size (1 to 10 microns) at most there would only be one or two slip bands capable of being accommodated for the stresses utilized.

2) Strains as high as 2 to 4 percent at the lower temperatures do not lead to discernible fine slip. Apparently the individual slips are so fine, and so well distributed, that the traces are poorly identifiable even on polished surfaces at relatively high magnifications.

3) Deformation at elevated temperatures is also characterized by the formation of fine slip lines on the surface. Again, slip bands are not observed, but it is much less probable that slip bands would be found in high temperature tests, in view of the fine grain size and the much lower stresses required.

4) Perhaps the most interesting aspect of high temperature creep deformation is the apparent absence or severe inhibition of grain boundary sliding and migration. Only in rare instances is there some evidence of small amounts of grain boundary migration, and exceedingly limited evidence of grain boundary shear. On average, the free grain boundary lengths between pinning oxide particles are so short that the unit shears would be extremely small and difficult to observe. On this basis, it is more likely that evidence of grain boundary migration would be present, and this is indeed the case.

5) Subgrains are observed after extensive deformation in high temperature creep of oxide dispersed Fe-BeO alloys.

6) While it is probable that the presence of a fine dispersion of BeO in alpha iron may lead to a decreased transition for brittle fracture, these Fe-BeO alloys undergo cleavage fracture at 77°K. This cleavage can be initiated by or superceded by ductile modes of fracture in the same regions.

7) Except for the cleavage type fracture in Fe-BeO alloys at 77°K, all of the fractures of the face-centered-cubic metals at 77°K, and all of the alloys at room temperature, showed ductile modes of fracture. The usual dimpled appearances in the fracture faces were abundantly evident. There appears to be evidence of void formation at the interface between the oxide dispersoid and the matrix. Such void nucleation appears to be associated preferentially with the flat surfaces of the larger, plate-like oxide particles.

8) High temperature fractures were observed to be both transgranular and intergranular, depending on the temperature and strain rate of the test. In the higher strain rate tests, many of the fractures appear to be transgranular; in the longer time, lower strain rate tests, the fractures tend to be intergranular. In particular, the Fe-BeO alloys, with a well defined ferritic grain structure, showed both types of fractures, with the fractures sharply intercrystalline in the longer time tests at 1200°F. The fractures occur on short grain boundary segments which are pinned by oxide particles, on grain boundaries which are oriented at favorable shear angles to the specimen axis. Fractures are not observed on short transverse boundaries or on the long axial grain boundaries. The short cracks on favorably oriented boundary segments, grow by shear at a later stage along the interconnecting axial boundaries. Fractures generally progress in a normal direction to the strain axis, not unlike that observed in conventional alloys.

(9) Extensive stress relaxation tests were run, from which activation volumes were calculated. The activation volumes for the oxide dispersed alloys are quite similar to those for the comparable pure metals or simple alloys, whether determined at 77°K, 20°C, or at elevated temperatures.

The net conclusion from the studies of deformation and fracture modes, supplemented by the activation energy calculations from stress relaxation tests, is that the oxide dispersed materials do not deform or fracture in a different manner than do more conventional alloys. The differences are not differences in kind, but in degree. Thus one sees less of slip bands and very much more of fine slip. In part, this is due both to the fine oxide dispersion, and to the very fine grain size. When conditions are correct for cleavage fracture, cleavage fractures take place in a conventional manner.

Grain boundary sliding and migration can occur, but the extent to which they do occur is extremely slight in view of the short range pinning of the boundaries by oxide particles. This restricts grain boundary sliding to short distances, which are incapable of being added up into large shears at either end of the grain boundary. These grain boundaries ultimately undergo intercrystalline cracking, and lead to intercrystalline failure under appropriate conditions of temperature and strain rate. The non-equilibrium grain structures, which deviate sharply from usual polygonal shapes, consist of sharply angular boundaries with jagged transverse boundary sections; this led to the necessary conditions for restricted grain boundary shear.

Except for the cleavage failures of Fe-BeO alloys at 77°K, and the intergranular failures in high temperature tests, the fractures of the other materials are typically ductile with normal dimpling.

E. Internally Oxidized, Alloyed, Nickel-BeO Materials

In view of the success achieved with internally oxidizing iron-beryllium alloys, equally fine-grained powders of nickel alloys will be internally oxidized in an effort to try to produce structures which will result in significant strength superiority and high temperature stability compared to current oxide dispersed nickel and nickel-base alloys.

A series of nickel-beryllium and alloyed nickel-beryllium alloys have been ordered in powder form; these powders will be attrited to -44 micron powders in most cases, and to sub-micron powders in other cases. Even in the presence of relatively large amounts of alloying elements, it should be possible to oxidize the beryllium in the nickel matrix to BeO.

It is also planned to make comparisons in several instances between products produced with low extrusion ratios followed by extensive cold worked, versus those produced by hot extrusion at a high extrusion ratio, without subsequent cold work. Basically we feel that these processing treatments result in two different classes of alloys, the behaviors of which might be expected to be significantly different.

II. THE SPLAT COOLING PROCESS FOR ALLOY DEVELOPMENT

A. Splat Cooling on a Continuous Basis

We are awaiting receipt of the desired high purity Al-Si alloy remelt stock, at 3 to 4, 7 to 8, and 10 to 11% silicon (these materials are not available commercially and are being prepared from higher purity grade materials for our use). Additional trial runs with other materials have been made in the meantime:

1) A switch has been made to the aluminum alloy 2024 from the Pb-Zn alloy. Aluminum is much more difficult to atomize because of heavy oxide formation; nevertheless, excellent splat runs have been accomplished, and a switch to the Al-Si alloys should not present unusual problems.

2) The atomization guns have been modified further; the liquid metal updraw tube is now being heated during the atomization run to avoid heavy skull formation at the lip of the gun.

3) An enclosure has been built around the rotating quench wheel to deflect particles which are not quench impacted against the rim of the wheel. Higher yield of more uniform splat flakes is being achieved without entrainment of more slowly cooled particles.

Several pounds of 2024 alloy were produced as splat cooled flake and separated in terms of two flake sizes. Both were cold compacted, canned, and extruded cold in the first experiments. A density of about 92% of theoretical was achieved, which is promising but not adequate. A new lot of material will be extruded at about 150°C to try to achieve higher density, followed by further rolling or swaging, if necessary, to full density.

The first lot of 2024 shows dendrite sizes between 10 and 40 microns, a size which is of interest for purposes of mechanical property study.

During the next six months it is expected that both the series of 3 Al-Si alloys will be evaluated for dispersion strengthening benefits, and the 2024 alloy will be compared to conventionally produced material (ingot practice). Several quench rates are planned for production of powders in addition to the one which the current experimental set-up will allow in the initial trials.

B. Splat Cooling of Al-Cu, Al-Fe, Al-Ni, and Al-Pd Alloys

A number of very interesting and valuable findings have resulted from recent studies of splat cooled aluminum binary alloys. One of the most interesting is the highly beneficial effect of doing the splat cooling under an inert gas or partial vacuum. As reported in the last semi-annual report, very thin splat cooled, aluminum alloy foils, atomized in an air atmosphere, reacted extremely rapidly with the high sulfur content of the winter atmosphere in the Boston area. Accordingly, splat cooling was performed in a protective atmosphere. A high beneficial side effect was the observation that more efficient splat cooling resulted from use of the non-oxidizing atmospheres. The splatted liquid particles were much finer, and the oxide skin much thinner.

In the Al-Cu system, whereas the maximum solubility of Cu at cooling rates of about 10^8 °C/sec was about 10-11% when splatting in air, the solubility increase is now indicated to be nearer 18% under conditions of a protective atmosphere. Similar benefits were observed with the other binary aluminum-base alloys; the latest results are shown in Table VIII.

TABLE VIII

Metasolubilities of Aluminum-Transition Metal Alloys Rapidly Quenched (Splat Cooled) in an Argon Atmosphere* (in atomic percent)

System	Maximum Equilibrium Solubility	Equilibrium Solubility at room temperature	Eutectic comp.	Maximum Solubility observed to date	Maximum Projected solubility limit (1)
Al-Fe	0.025% at 655°C	<0.003 at. %**	0.9% Fe	4.1%	<5%
Al-Ni	0.023% at 640°C	<0.003 at. %**	2.7% Ni	1.0%	<3%
Al-Cu	2.5% at 548°C	<0.04-0.08 at.% at 250°C	17.3% Cu	~16.0%	<18% (2)
Al-Pd	none observable by lattice parameter measurements	none observable	7.5% Pd	6.75%	<8% (2)

* The measured metasolubilities of Al-transition metal alloys rapidly quenched in an argon atmosphere differ significantly from those of alloys splat cooled in air. All diffraction patterns of Al splat cooled in air show at least one extraneous reflection, most probably attributable to a corrosion product. Recent observations suggest that the rapidity and degree of oxidation and corrosion of ultra-fine foils of Al during the splat process is sufficient to decrease the cooling rate and cause the observed reduction in the measured metasolubilities.

** The values for equilsolubility of Al-Fe, Al-Ni are given as <.003 at. % as these are the min. measured. Both are at 500°C.

(1) The maximum projected solubility limit is based on the lowest alloying composition that (1) a 2 phase splat shows by X-ray diffraction techniques, or, (2) for which a change in slope of the lattice metastable parameter vs. composition curve is observed.

(2) It is reasonable to expect the maximum metasolubilities of Al-Cu and Al-Pd to occur at or very near the eutectic composition.

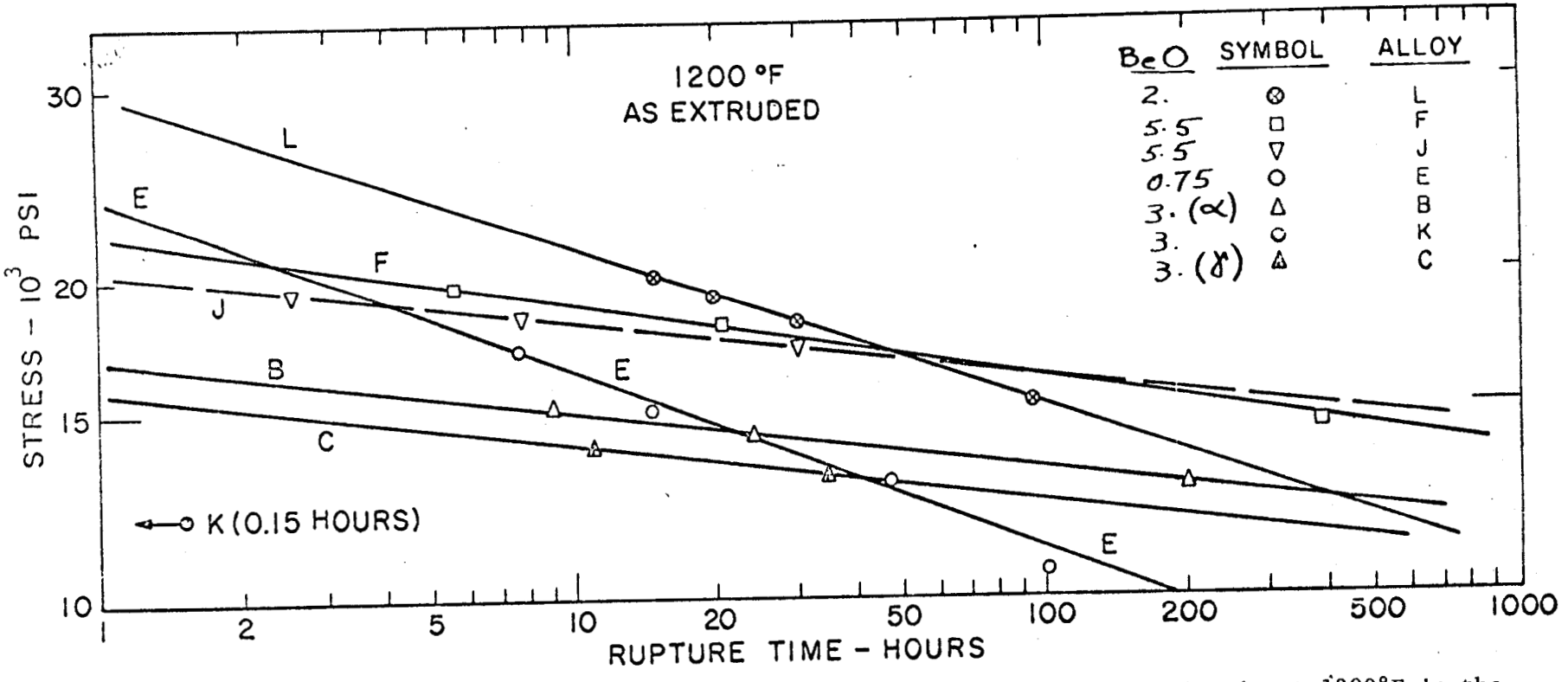

Fig. 1: Plot of log stress vs. log rupture time for Fe-BeO alloys tested in air at 1200°F in the as-extruded condition. Alloy L contains 0.7% in solution; alloy K is an Fe-4.7% Ni alloy.

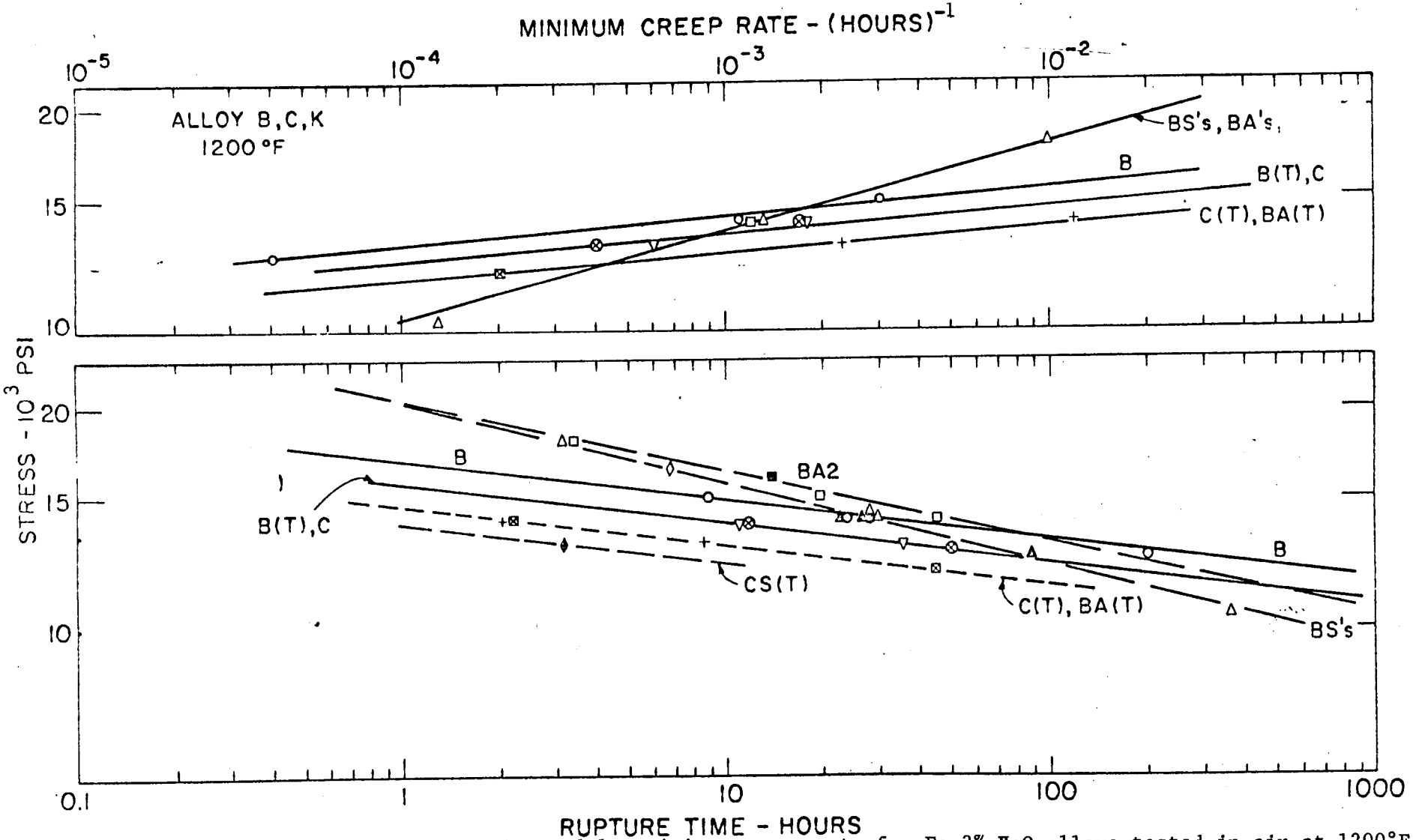

Fig. 2: Log stress vs. log rupture time and log minimum creep rate for Fe-3% BeO alloys tested in air at 1200°F, for various treatments:

B: as-extruded, alpha. C: As-extruded, gamma. B(T): alloy B annealed 1.5 hr,1720°F.

B(A),B(S): alloy B, cold worked. C(T): Alloy C annealed, 1.5 hr,1720°F. BA(T): alloy B + cold work, annealed 1.5 hr., 1720°F.

CS(T): alloy C + cold work, annealed 1.5 hr., 1720°F.

Fig. 3: Log stress vs. log rupture time, with extrapolations, for Fe-BeO alloys F (5.5% BeO) and B (3.0% BeO) compared to best ferritic stainless alloy H-46, and type 430; air tests at 1000, 1200, and 1400°F.

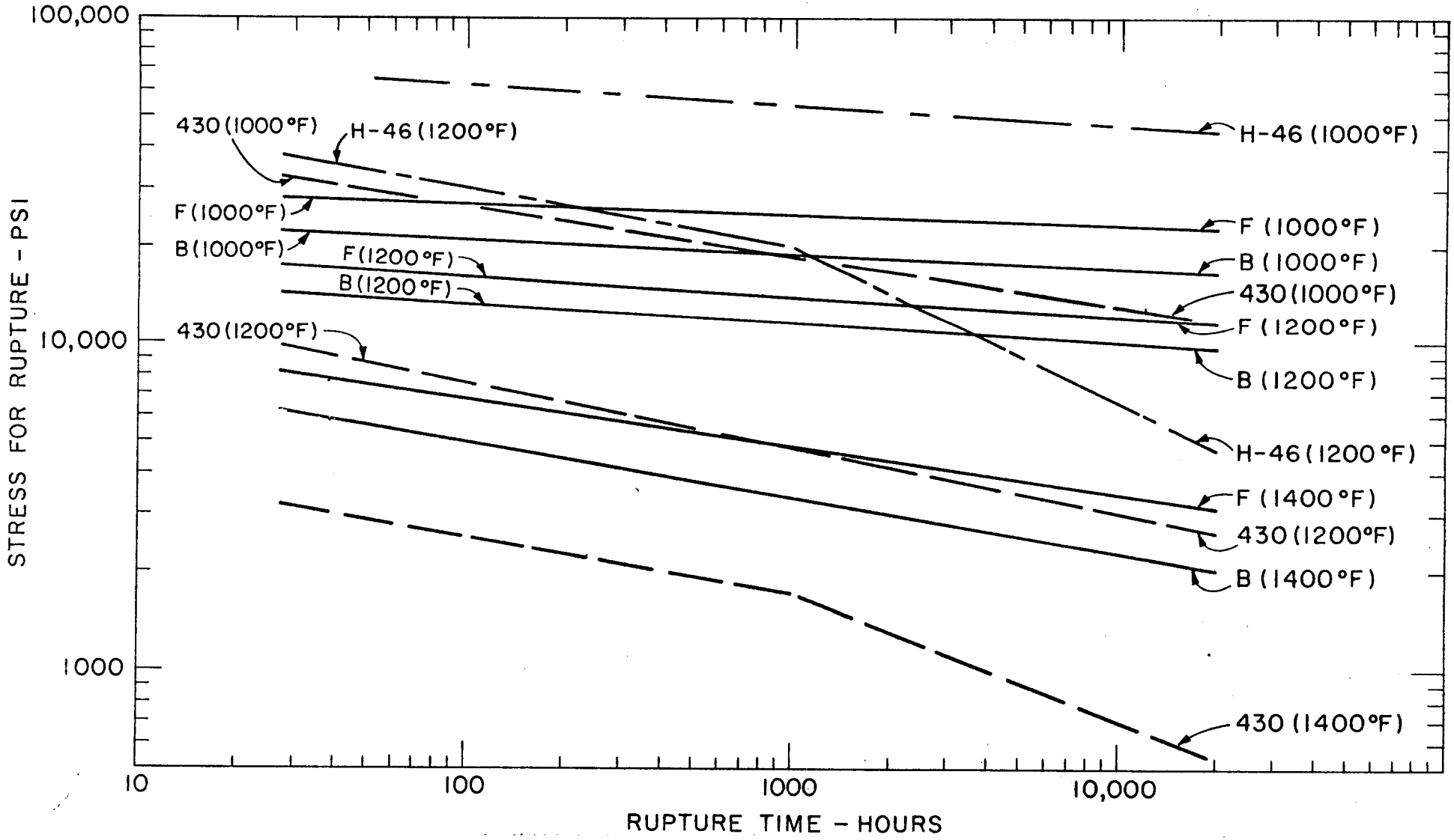

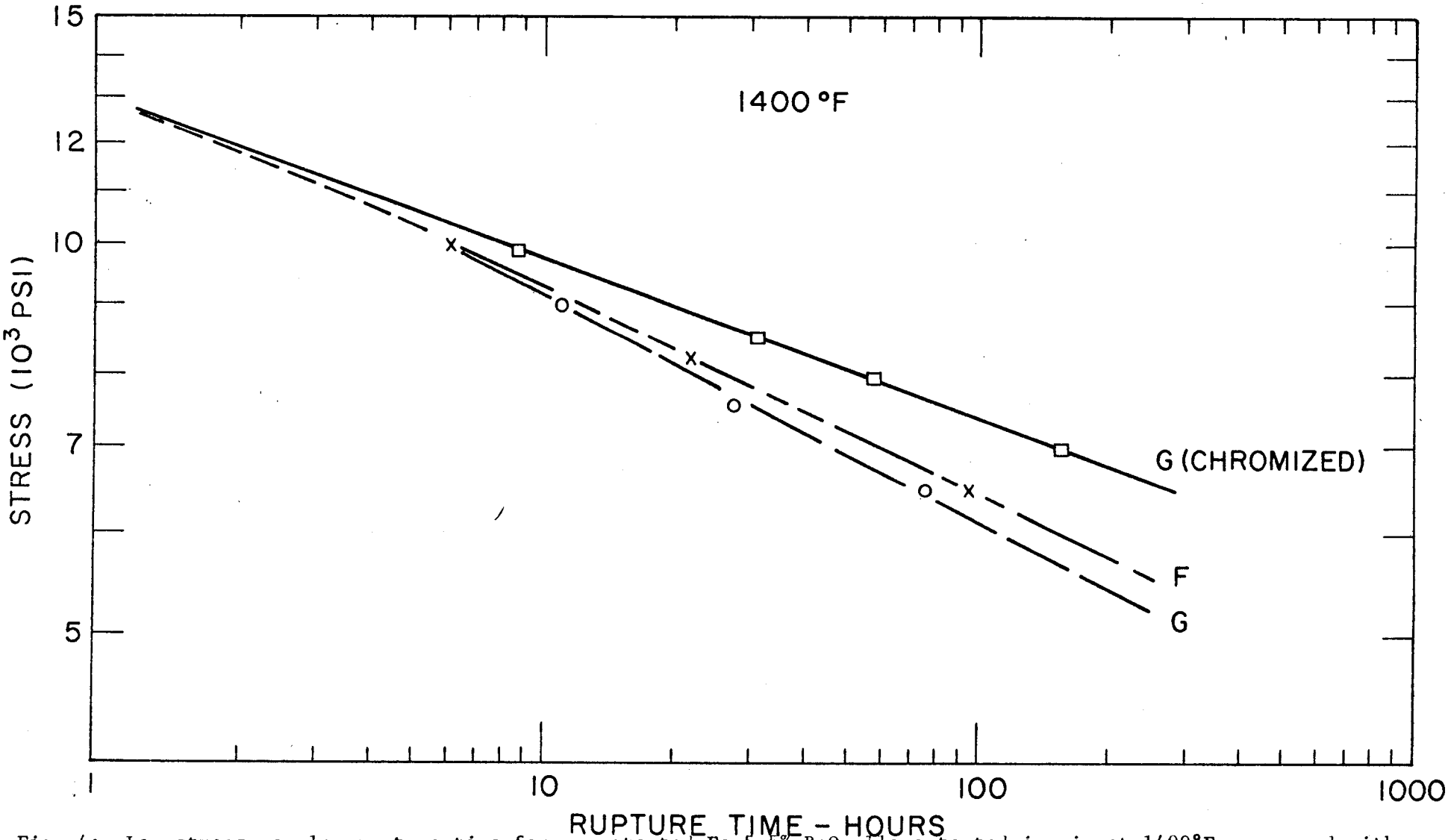

Fig. 4: Log stress vs. log rupture time for unprotected Fe-5.5% BeO alloys tested in air at 1400°F, compared with alloy G in the chromized condition.

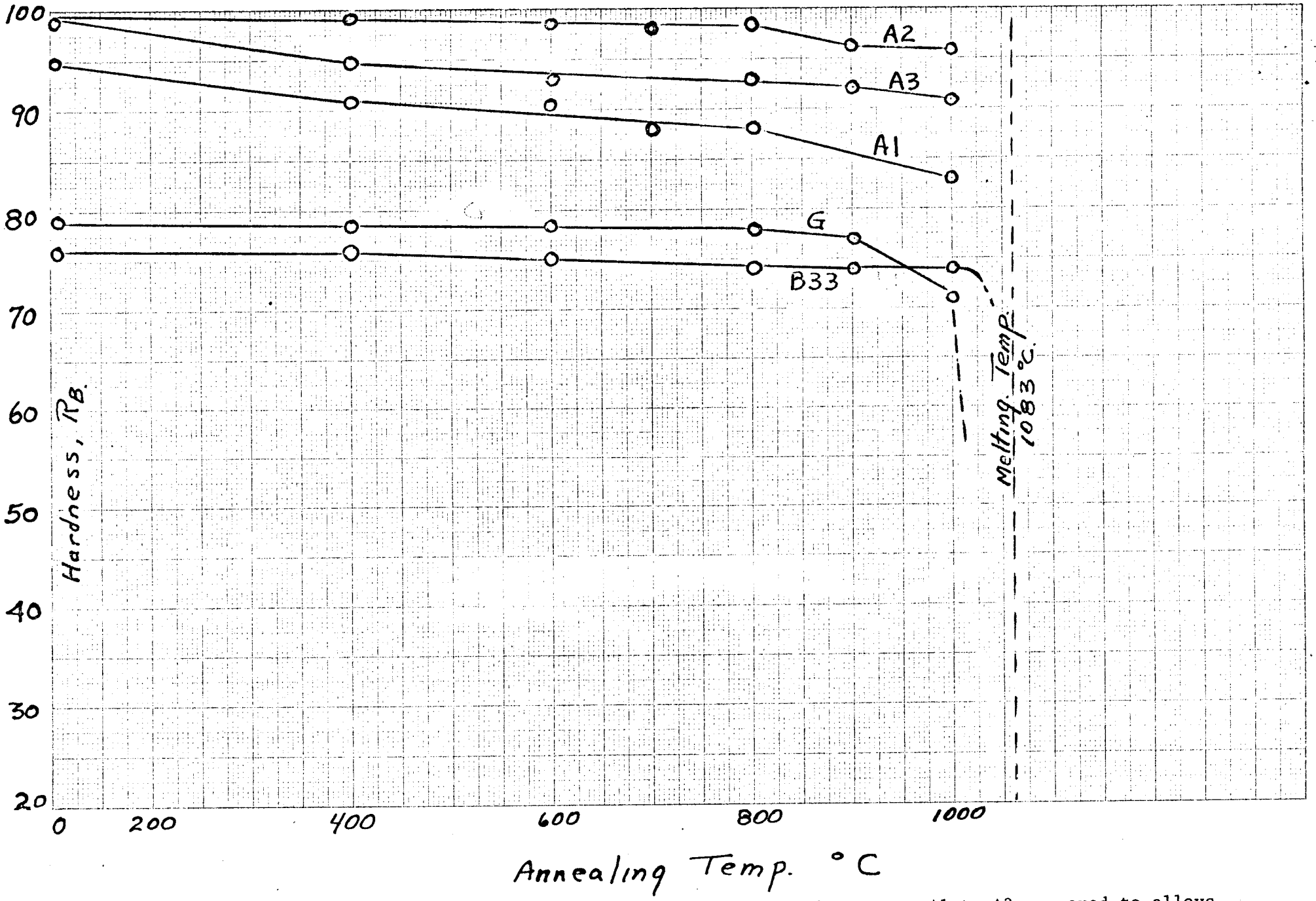

Fig. 5: Room temperature hardness vs. one hour annealing temperature for curves A1 to A3 compared to alloys G and B-33.